Amidoxime-Functionalized Covalent Organic Framework as Simultaneous Luminescent Sensor and Adsorbent for Organic Arsenic from Water

Hui Chen[a], Wanlu Liu[a,b],Long Cheng[c], Maria Meledina[d,e] Rik Van Deun[b], Karen Leus[a], and Pascal Van Der Voort[a*]

a COMOC-Center for Ordered Materials, Organometallics and Catalysis, Department of Chemistry, Ghent University, Krijgslaan 281-S3, 9000 Ghent, Belgium.

b L^3-Luminescent Lanthanide Lab, Department of Chemistry, Ghent University, Krijgslaan 281-S3, 9000 Ghent, Belgium.

c School of Chemistry and Chemical Engineering, Southeast University, Nanjing 211189, P. R. China.

d RWTH Aachen University, Central Facility for Electron Microscopy, D-52074, Aachen, Germany.

e Forschungszentrum Jülich GmbH. Ernst Ruska-Centre (ER-C2). D-52425, Jülich, Germany.

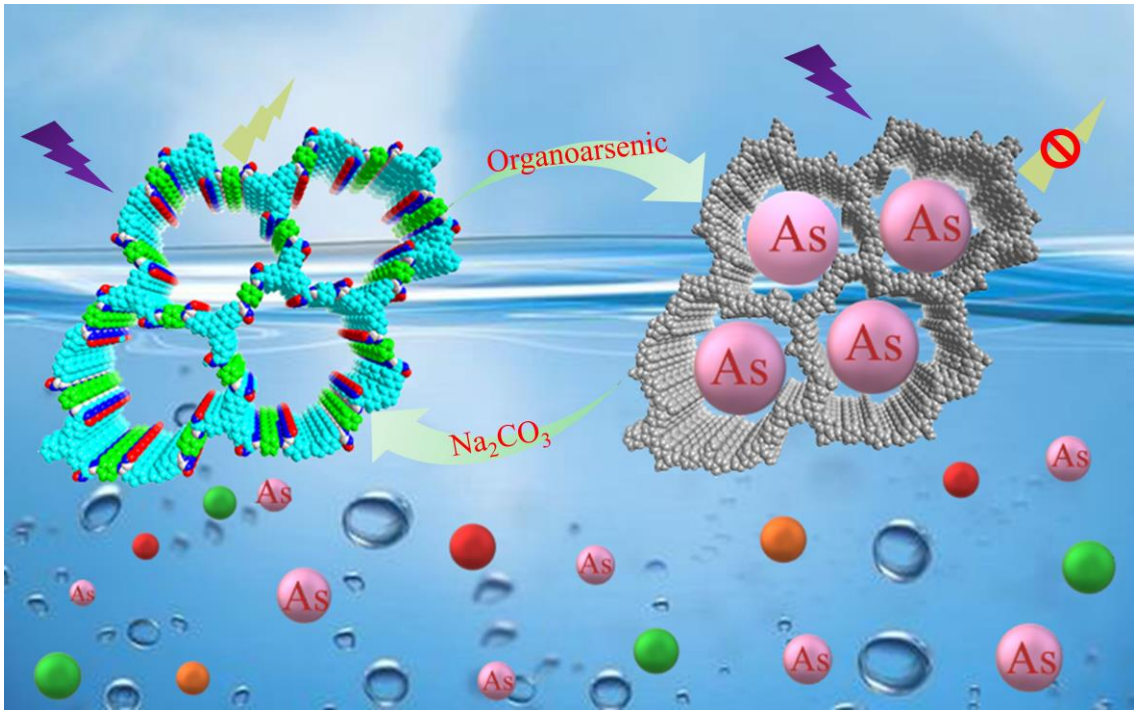

Abstract

Organoarsenic compounds are widely used as feed additives in the poultry industry. However, the release of organoarsenic-containing wastewater can cause serious poisoning to the ecosystem. For this reason, detection and adsorption of organic arsenic from wastewater is crucial but also very challenging. Here, the use of covalent organic frameworks (COFs) as fluorescence sensors and adsorbents for the detection and adsorption of organic arsenic from water has been investigated for the first time. Two isoreticular crystalline and highly porous sp^2 carbon-conjugated COFs were synthesized, and amidoxime-functionalized *via* post-synthetic modification (PSM). The long-range order and π-conjugated system ensure that both COFs act as fluorescent sensors for detecting the representative organic arsenic, roxarsone (ROX). The fluorescence quenching efficiencies of ROX on both COFs are over 98%. The limits of detection (LOD) for ROX by both COFs are estimated to be 6.5 nM and 12.3 nM. Additionally, the regular pores and the abundantly decorated amidoxime moiety exhibit extraordinary accessibility, which facilitates the adsorption of ROX. High adsorption capacities were obtained for both materials which amounts are up to 732 and 787 mg/g. After five times of recycling, a negligible decrease in the adsorption capacity was noted, which reveals the excellent regeneration ability of those two amidoxime-functionalized COFs. These results indicate that the state-of-the-art sp^2 carbon conjugated amidoxime-functionalized COFs exhibit a high potential for the practical detection and adsorption of organoarsenic compounds from wastewater.

Introduction

Arsenic is a confirmed toxic carcinogen for all life forms. Long-term exposure to arsenic leads to various health problems for humans, such as cancer and skin lesions, cardiovascular disease, diabetes, negative impacts on cognitive development, and even increased deaths of infants[1]. Scientists have made considerable efforts to detect and remove arsenic from the ecological environment. Nevertheless, most of these studies were focused on inorganic arsenic species, while the organic form of arsenic has received considerably less attention[2]. Organoarsenic compounds have been widely used in the poultry industry as a feed additive to promote weight gain, prevent dysentery, control intestinal parasites, and as antibacterial agents [3]. Unfortunately, the high usage of organoarsenic compounds has caused great harm to nature. When water-soluble organoarsenic compounds enter into the ambient environment, they are easily transferred into the highly toxic inorganic arsenite (As (III)) and arsenate (As(V)) *via* biodegradation or/and chemical oxidation. This leads to pollution of land and groundwater[4]. Subsequently, they can accumulate in plants and eventually enter the human food chain, and finally the human body[5]. Roxarsone (4-Hydroxy-3-nitrophenyl arsonic acid, abbreviated as ROX, **Scheme 1**) as a representative organoarsenic compound is the most widely applied feed additive[3a, 4a]. The amount of ROX used in feed additives has increased over the past years and is excreted in manure, after which it subsequently accumulates in the litter, where it can reach arsenic concentrations up to 1000 μg/kg. This value far exceeds the 0.5 ppm safety standard set by the World Health Organization (WHO)[2d]. So far, the utilization of porous adsorbents to remove ROX residues is considered to be the cheapest and most effective treatment approach. A variety of adsorbents have been developed to efficiently remove ROX from water, such as multi-walled carbon nanotubes (MWCNTs)[6], porous-carbon materials[7],

chitosan-based copolymers[8], and metal-organic frameworks (MOFs)[2b]. However, these materials possess some drawbacks such as slow sorption kinetics, limited selectivity, small pore volumes or pore sizes, complicated synthesis, as well as relatively low chemical and thermal stability. Therefore, the development of simple and inexpensive porous adsorbents to clean up ROX in water is of high importance. Additionally, the detection of ROX in wastewater is a precondition to the removal. Up till now, the detection of ROX still relies on various cumbersome large-scale instruments such as gas chromatography (GC)[9], inductively coupled plasma mass spectrometry (ICP-MS)[10], high-performance liquid chromatography (HPLC)[11], and so on. Consequently, the development of new detection methods that can be used in this field is highly desired. Fluorescence sensing has attracted considerable attention because of the strong visual recognition ability, fast response, and high selectivity[12].

In recent years, the investigation of COFs became a very active research area because of their remarkable features, including large specific surface areas, π-π stacking interactions, high chemical and thermal stability, long-range order, and hierarchically integrated building blocks[13]. Furthermore, the stable structure and prearranged sites of COFs allow the introduction of functional groups onto the pore wall via post-synthetic modification (PSM), which paved the way towards various functional COFs[14]. Their light-harvesting and energy transition capabilities make them promising luminescent sensing materials[15]. The structure of ROX (see **Scheme1**) possesses a $-NO_2$ and a $-AsO(OH)_2$ group. This $-NO_2$ group can efficiently quench the fluorescence of COFs[16], and the $-AsO(OH)_2$ group can form strong hydrogen bonds with the N, O, and H containing groups. For this reason, COFs can function simultaneously as a fluorescence sensor and as an adsorbent to detect and remove ROX.

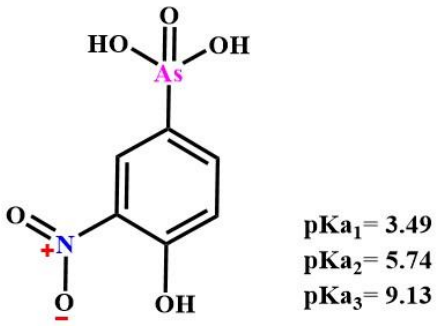

Scheme 1: Chemical structural formula and pKa values of roxarsone

Herein, we designed and synthesized two isoreticular 2D amidoxime-functionalized COFs, denoted as AO-COF-ben and AO-COF-tri, respectively (**Scheme 2, Figure 1a and Figure 1b**). As the amidoxime group is susceptible to react with the building units during the COF construction process, a PSM strategy was employed to build these amidoxime-functionalized COFs. Firstly, two cyano groups assembled COFs, CN-COF-ben and CN-COF-tri, were synthesized. Then, those cyano groups assembled COFs were amidoximated by treatment with hydroxylamine to afford the amidoxime-functionalized AO-COF-ben and AO-COF-tri.

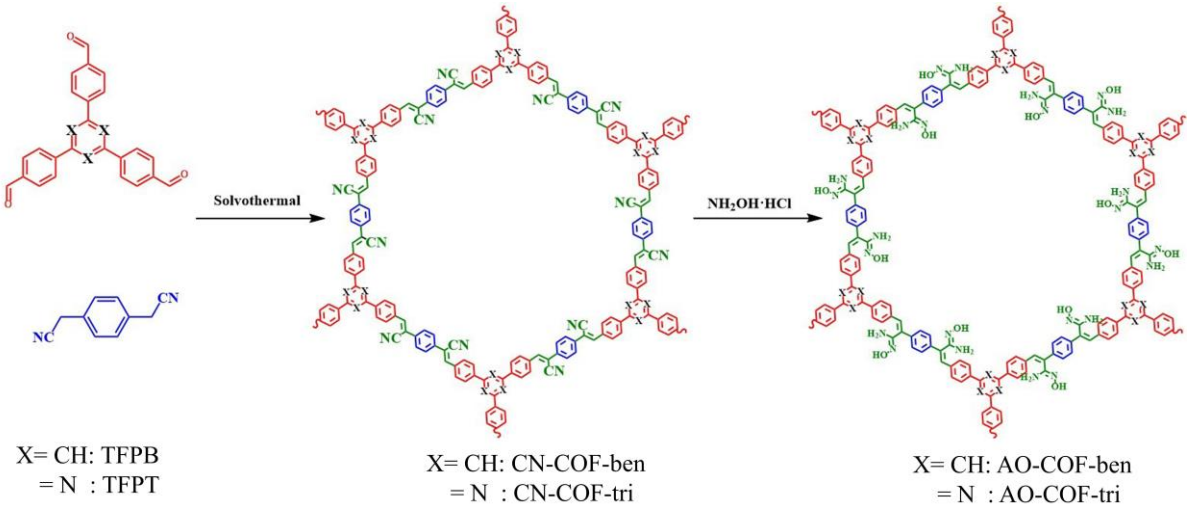

Scheme 2: Synthesis and structures of the AO-COF-ben and AO-COF-tri.

Results and discussion

The chemical structure of the pristine CN-COF-ben and CN-COF-tri was confirmed by means of Fourier-transform infrared spectroscopy (FT-IR). As shown in **Figure 1e**, the vibration observed at 2212 cm^{-1} corresponds to the -CN group, indicating that the -CN group survived the condensation reaction. The signal observed at 3027 cm^{-1}, can be assigned to the C-H stretching vibration of -C=C-H, which shows the formation of C=C bonds. This implies the successful condensation of the monomers and the formation of the framework. Upon the treatment with hydroxylamine, the -CN group stretching band disappeared, and new vibrations at 1646 cm^{-1} (C=N) and 924 cm^{-1} (N-O) have appeared, which originates from the amidoxime group. These vibrations demonstrate the successful amidoxime-functionalization of the AO-COF-ben and AO-COF-tri. The crystalline structures of the pristine COFs and the amidoxime-functionalized COFs were determined by powder X-ray diffraction (PXRD) analysis (**Figure 1c and Figure 1d**). For CN-COF-ben and CN-COF-tri, the experimental PXRD patterns match well with the reported pattern[17], which shows that an eclipsed AA stacking mode is preferred over a staggered AB stacking. The PXRD patterns of the AO-COF-ben and AO-COF-tri are similar to that of the pristine COFs, indicating that the crystallinity of the COFs is preserved upon the amidoxime-functionalization. The morphology of AO-COF-ben and AO- COF-tri were examined by scanning electron microscopy (SEM) and transmission electron microscopy (TEM). As shown in **Figure S1**, rough rods are observed and no changes in the shape are detected after post-modification with hydroxylamine. This means that the framework integrity was preserved during the chemical post-modification. The surface area and permanent porosity of the pristine and amidoxime-functionalized COFs were evaluated by Ar adsorption-desorption experiments at 87 K (**Figure 1f**). The Brunauer-Emmett-

Teller (BET) surface area decreased from 393 $m^2 g^{-1}$ and 378 $m^2 g^{-1}$ for CN-COF-ben and CN- COF-tri to 218 $m^2 g^{-1}$ and 203 $m^2 g^{-1}$ for AO-COF-ben and AO-COF-tri, respectively. The pore-size distribution (PSD), presented in **Figure S2**, shows that the main pore size is 23.4 Å for CN-COF-ben and 34.6 Å for CN- COF-tri. These pores are assigned to AA stacking motifs. As the Knoevenagel condensation is not perfectly reversible, stacking faults in the structure cannot be completely avoided. Therefore, an additional smaller pore with sizes of 14.1 and 29.2 Å appear in CN-COF-ben and CN-COF-tri, respectively, which are assigned to the random occurrence of AB stacking faults within the AA stacked structure[17b, 18]. After amidoxime functionalization, the pore size was slightly decreased (12.8 and 21.3 Å for CN-COF-ben and 27.6 and 32.3 Å for CN- COF-tri). From these observations, it is clear that, although the interior cavities of the AO-COF-ben and AO-COF-tri are partially occupied by the amidoxime moiety, the AO-COF-ben and AO-COF-tri structures still exhibit a permanent open structure, ensuring a good diffusion of the analytes or adsorbates to the amidoxime functional groups.

Besides the permanent porosity, the thermal and chemical stability are also very important for their practical application as fluorescence sensors and adsorbents. As indicated in **Figure S3**, the thermogravimetric analysis (TGA) shows that both AO-COF-ben and AO-COF-tri possess excellent thermal stability. Both of them are stable up to 350 °C under an air atmosphere. Additionally, AO-COF-ben and AO-COF-tri exhibit remarkable chemical stability in boiling water, common organic solvents, strong acid (12 M HCl aqueous), and strong base (12 M NaOH aqueous). After soaking both AO-COF-ben and AO-COF-tri material in each of these media for 3 days, no change was observed in the PXRD pattern (**Figure S4**), indicating the high chemical stability of both COFs.

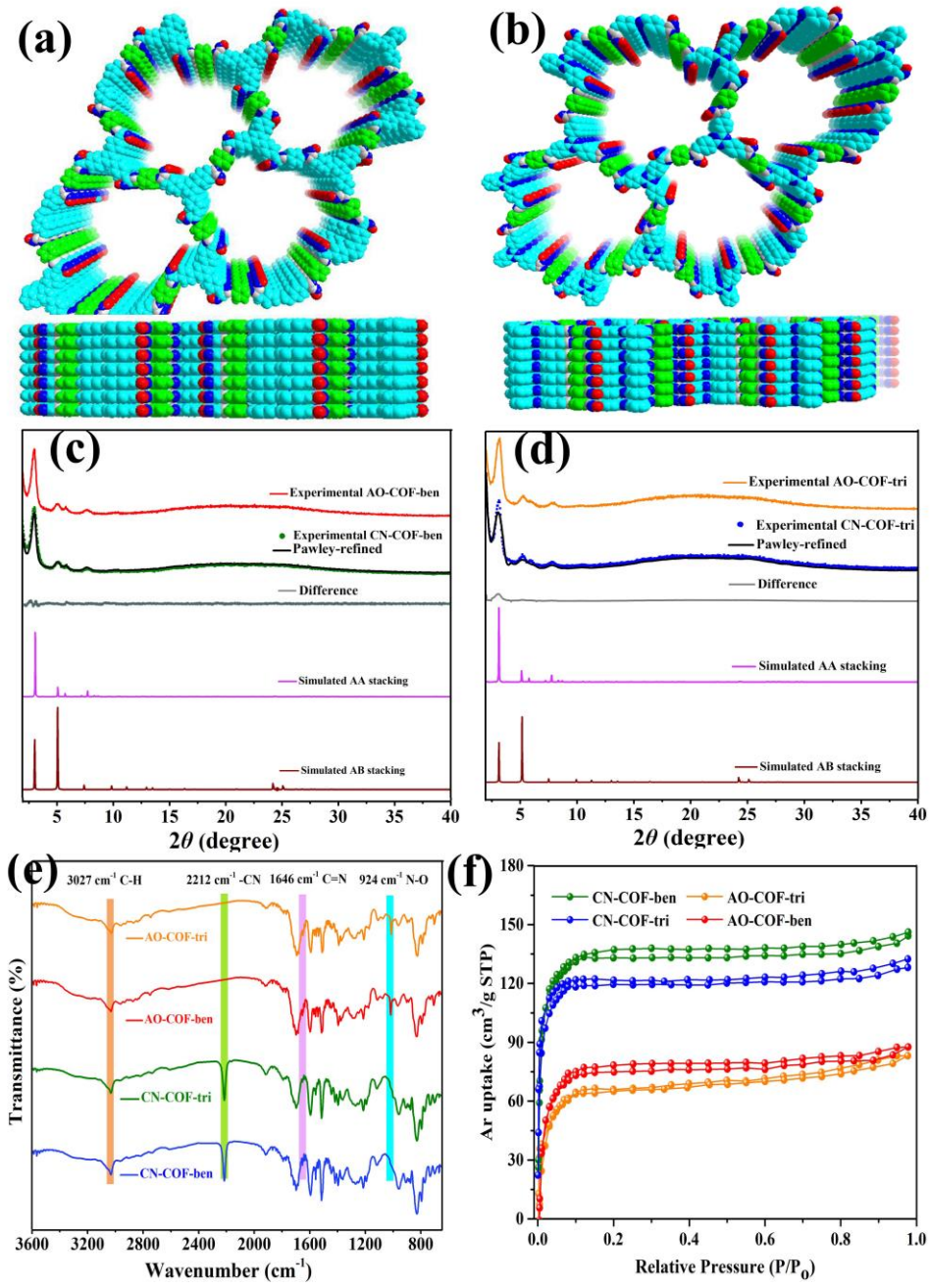

Figure 1. Side and top views of AO-COF-ben (a) and AO-COF-tri (b); PXRD pattern of AO-COF-ben (c) and AO-COF-tri (d); (e) FT-IR spectrum of CN-COF-ben, CN-COF-tri, AO-COF-ben, and AO-COF-tri; (f) Ar adsorption/desorption isotherms of CN-COF-ben, CN-COF-tri, AO-COF-ben, and AO-COF-tri at 87 K.

Detection of organic arsenic. Due to the long-range order of the crystalline AO-COF-ben and AO-COF-tri materials, the π-conjugated system is considerably enhanced. Compared to an σ-σ^* transition, the π–π* transition is easier because of the lower energy difference (ΔE). As a result of this, π-conjugated systems undergo electronic excitations

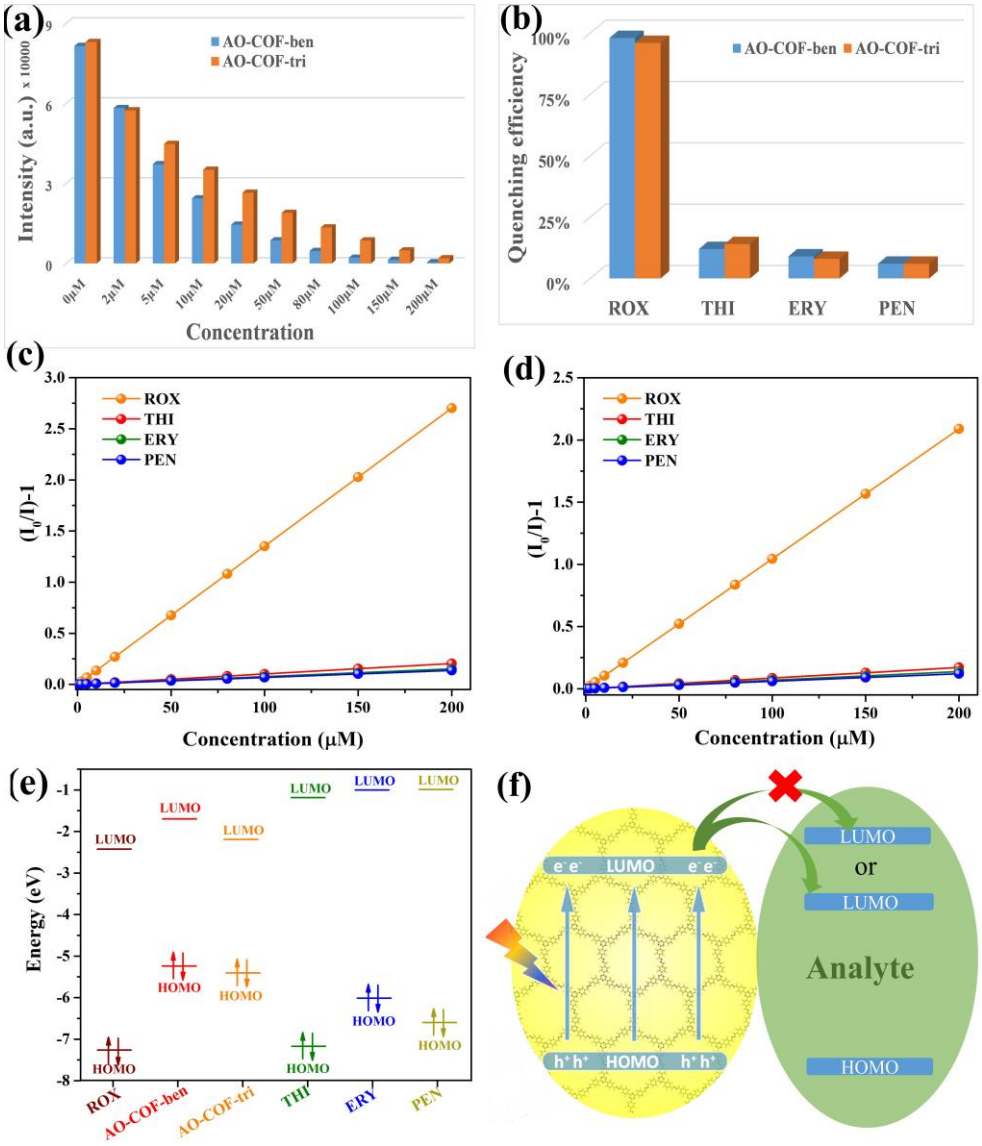

Figure 2. (a) Fluorescence changes of AO-COF-ben and AO-COF-tri after adding various concentrations of ROX; (b) Fluorescence quenching efficiency of AO-COF-ben and AO-COF-tri by different analytes at RT; Stern–Volmer plots of AO-COF-ben (c) and AO-COF-tri (d); (e) HOMO and LUMO energies for tested analytes and AO-COF-ben and AO-COF-tri; (f) The scheme of electron transfer phenomena via PET mechanism.

more easily than their saturated counterparts [19]. Additionally, the efficient π-electron communication along both the x and y directions of sp^2 carbon-linked COFs results in enhanced π-delocalization over 2D networks and greater emission activity[20]. In this way, their application as a fluorescence sensor for detecting ROX in water was explored.

The ability of AO-COF-ben and AO-COF-tri to detect ROX through fluorescence quenching was investigated by adding various concentrations of ROX into a 50 mg/L

aqueous suspension of these two amidoxime-functionalized COFs. Upon excitation at 365 nm, AO-COF-ben and AO-COF-tri show a single emission peak at 513 nm and 522 nm, respectively (**Figure S5**). Both amidoxime-functionalized COFs show an excellent detection performance towards ROX, a significant decrease of the fluorescence intensity was observed upon increasing the concentration of ROX (**Figure S6**). More specifically, when the concentration of ROX was increased from 0 μM to 200 μM, the fluorescence intensity decreased more than 200-fold (**Figure 2a**). The fluorescence quenching efficiencies of AO-COF-ben and AO-COF-tri towards ROX are 97% and 98%, respectively (**Figure 2b**). The fluorescent quenching efficiency can be quantified by the Stern-Volmer equation (SV): (I_0/I)-1 = K_{sv}[Q]. As shown in **Figure 2c and Figure 2d**, the SV plots for both COFs show a good linear relationship for the ROX (R^2 = 0.996 and 0.995, respectively), which implies that there is a static or dynamic quenching process[21]. The Stem-Volmer constant (K_{sv}) of AO-COF-ben and AO-COF-tri for ROX are 13513 M^{-1} and 10448 M^{-1}, respectively. Based on the K_{sv} values and the standard deviations (S_b) for three repetitions of fluorescent measurements from the blank solutions, LOC for AO-COF-ben and AO-COF-tri towards ROX were calculated to be 6.5 nM and 12.3 nM, respectively. These values are much lower than the 0.5 ppm ROX content (corresponds to 19 nM) safety standard set by WHO.

It should be mentioned that in the livestock farm wastewater, many other organic molecules are co-existing, such as thiamphenicol (THI), erythromycin (ERY), penicillin (PEN), *etc.* (**Scheme S1**). To check the selectivity of AO-COF-ben and AO-COF-tri towards ROX, these organic molecules were employed as interfering agents and added to the AO-COF-ben and AO-COF-tri suspension to record the corresponding fluorescent emissions intensity. As shown in **Figure S7 and S8**, when the concentrations of these interfering agents increased, no significant changes were

observed in the suspension fluorescence intensity. This means that they exhibit a poor fluorescence quenching efficiency (**Figure 2b**). The Stem-Volmer constant (K_{sv}) of AO-COF-ben for THI, ERY, and PEN are 856 M^{-1}, 693 M^{-1}, and 604 M^{-1}, respectively (**Figure 2c**) whereas the K_{sv} of AO-COF-tri for THI, ERY, and PEN are 1024 M^{-1}, 763 M^{-1}, and 683 M^{-1}, respectively (**Figure 2d**). These values are approximately 15 times lower than that of ROX. Additionally, upon the addition of the ROX aqueous solution (0.5 ml 200 μM) to the COFs suspension with the interfering agents, the fluorescence intensity dropped sharply and disappeared (**Figure S9**). All these results show that both the AO-COF-ben and AO-COF-tri exhibit high selectivity for the detection of ROX in the presence of the interfering agent. In order to simulate natural wastewaters, the water from different ecological environments was selected to replace the deionized water for ROX detection, including seawater, river water, and lake water. As shown in **Figure S10** and **Figure S11**, it is clear that the usage of water from various ecological environments has a negligible effect on the detection efficiency of AO-COF-ben and AO-COF-tri. Or in other words, these results show that the amidoxime-functionalized COFs can be used in real natural waters. Another important aspect of its practical implementation is the recyclability of the fluorescence sensor. After the first usage, the COFs were washed with 1M Na_2CO_3 aqueous solution and used for 4 additional cycles. As seen from **Figure S12**, the fluorescence quenching efficiency of both amidoxime-functionalized COFs towards ROX remained unchanged during these successive cycles, demonstrating their high recyclability and stability for sensing.

In order to better understand the origin and mechanism of the fluorescence sensing and high selectivity towards ROX, the molecular orbits (MO) of both AO-COF-ben and AO-COF-tri were calculated (**Figure S13**). When the lowest unoccupied molecular orbital (LUMO) of the COFs lies on higher energy than that of the analytes,

the excited COF acts as an electron donor and the analyte as an electron acceptor. Upon excitation, there is a driving force to maintain the excited electron transfer from the COFs to the analyte, which results in fluorescence quenching[22](**Figure 2f**). As shown in **Figure 2e** and **Table S1**, the LUMO energy levels of THI, ERY, and PEN are higher than the LUMO energy levels of the AO-COF-ben and AO-COF-tri. This means that the electron jump from the excited COFs to these analytes is thermodynamically forbidden, resulting in a poor fluorescence response. In contrast, the LUMO energy level of ROX is situated below the LUMO level of AO-COF-ben and AO-COF-tri. So, there exists a photoinduced electron transfer (PET) process in the detection of ROX, which leads to high efficiency and fast detection of ROX for both COFs. Based on these calculations, it's clear that the origin and mechanism of the fluorescence sensing and high selectivity towards ROX can be explained by the donor-acceptor electron-transfer mechanism. Additionally, from the MO calculations (**Figure S13**), we can see that the highest occupied molecular orbital (HOMO) is associated with the π-bonding orbital from the hexagonal ring, whereas the LUMO is mainly associated with the π-antibonding orbital in both AO-COF-ben and AO-COF-tri. Due to the fact that the electronegativity of the N atom is larger than the C atom, the electron transfer from the LUMO of AO-COF-tri to the LUMO of the analyte becomes slower than that of AO-COF-ben[21]. This explains why the detection efficiency of AO-COF-ben is better than that of AO-COF-tri for ROX.

Adsorption of organic arsenic. Considering the high porosity, excellent stability, and abundant amidoxime functional groups (~3.57 mmol/g), AO-COF-ben and AO-COF-tri have also been investigated as adsorbents for the adsorption of ROX in water. The adsorption isotherms of ROX on AO-COF-ben and AO-COF-tri are shown in **Figure3a**. In order to understand the interactive behavior between the amidoxime-

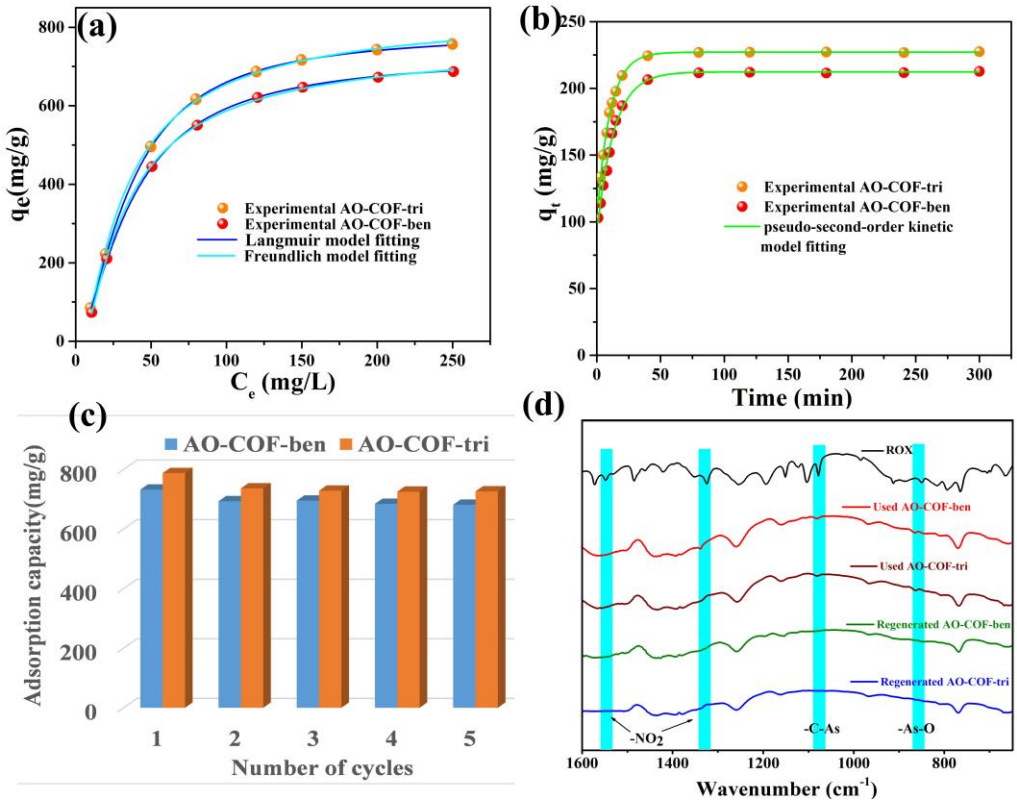

Figure 3. (a) Adsorption isotherms of ROX by AO-COF-ben and AO-COF-tri. (b) Adsorption kinetic curves of ROX by AO-COF-ben and AO-COF-tri. (c) Regeneration ability of AO-COF-ben and AO-COF-tri. (d) FT-IR spectrum of ROX, used AO-COF-ben and AO-COF-tri, regenerated AO-COF-ben and AO-COF-tri.

functionalized COFs and ROX during the adsorption process, two most commonly used isotherm models, the Langmuir and Freundlich model, were employed to fit the adsorption isotherm. As shown in **Table 1**, all the isotherms fitted well with both the Langmuir and Freundlich models. However, the R^2 values of the Langmuir model are higher than the Freundlich model, indicating that the Langmuir model is more suitable to explain the ongoing adsorption process. This suggests that a monolayer adsorption process on the amidoxime-functionalized COFs towards ROX is more likely and that the maximum adsorption corresponds to a saturated monolayer of solute molecules onto the adsorbent surface. Therefore, in the following discussion, the Langmuir fitting results of the COFs were chosen. The maximum adsorption capacities (q_m) are 732 mg/g and 787 mg/g for AO-COF-ben and AO-COF-tri, respectively. These values are higher

in comparison to other similar reported adsorbents (such as MIL-100-Fe[23], UIO-66[24], UIO-66-NH_2[25], **Details see Table S2**).

Table 1. Parameters for ROX adsorption on AO-COF-ben and AO-COF-tri when fitting the adsorption data using Langmuir and Freundlich isotherm models.

Model	Langmuir model			Freundlich model		
Samples	**k_L(L/mg)**	**q_m (mg/g)**	**R^2**	**k_F (mg^{1-n} L_n/g)**	**n**	**R^2**
AO-COF-ben	**0.046**	**732**	**0.994**	**19.19**	**1.25**	**0.963**
AO-COF-tri	**0.032**	**787**	**0.996**	**58.83**	**1.29**	**0.982**

Besides the adsorption capacity, the rate of ROX removal from water by the amidoxime-functionalized COFs was also investigated *via* adsorption kinetics. As shown in **Figure 3b**, the ROX adsorption for both amidoxime-functionalized COFs increases rapidly at the first stage and reaches 90% of its adsorption equilibrium within 15 min and 20 min, respectively. This is possibly caused by two factors: i) the large concentration gradient is a powerful driving force for ROX adsorption. ii) the abundant active sites present in the pores of the amidoxime-functionalized COF adsorbents, are favorable for the capture of ROX molecules from water. After the initial sharp increase, the adsorption process finally reaches its equilibrium after 20 min and 25 min for AO-COF-tri and AO-COF-ben, respectively. The slightly faster kinetics observed for the AO-COF-tri in comparison to the AO-COF-ben is probably the result of the planarity of the TFPT linker which leads to higher crystallinity of the AO-COF-tri and consequently results in a better long-range order arrangement of the active sites[26]. To further investigate these time-dependent adsorption changes for the two amidoxime-functionalized COFs adsorbents, the pseudo-second-order kinetic model was used to simulate the ROX adsorption on both COFs. In the pseudo-second-order kinetic model,

the rate-limiting step is the surface adsorption that involves chemisorption, where the removal from a solution is due to physicochemical interactions between the two phases and the number of active sites which determines the adsorption capacity[27]. As shown in **Figure 3b** and **Table 2**, the adsorption kinetics curves of ROX fitted well with the pseudo-second-order kinetic model with correlation coefficients of more than 0.99. This indicates that the adsorption of ROX on the two amidoxime-functionalized COFs is more controlled by chemical interactions than by physical adsorption. The adsorption rate constant (k_2) of AO-COF-ben and AO-COF-tri to ROX was calculated to be 0.24 and 0.32 g mg^{-1} min^{-1}, respectively. These high adsorption rates for ROX were adsorbed on AO-COF-ben and AO-COF-tri probably the result of the stronger chemical interactions observed between the amidoxime-functionalized COFs and the ROX molecules.

Table 2. Kinetic parameters of pseudo-second-order models for ROX adsorbed on AO-COF-ben and AO-COF-tri ($C_{initial}$ = 20 mg/L, T = 25 ◦C, pH=4)

	pseudo-second-order kinetic model		
	k_2 (g/mg*min)	q_e (mg/g)	R^2
AO-COF-ben	0.24	211.78	0.996
AO-COF-tri	0.32	227.28	0.999

Recyclability is an important aspect of an adsorbent. To demonstrate its reusability, the COF was washed at the end of the adsorption process with a 1 M Na_2CO_3 aqueous solution to desorb the ROX. As shown in **Figure 3c**. After five cycles of adsorption-desorption, the removal performance for both amidoxime-functionalized COFs decreased slightly, revealing the excellent regeneration ability. The slight decrease in adsorption performance may be due to the accumulation of tightly bounded ROX onto

the functional groups of the amidoxime-functionalized COFs. What's more, after five cycles, the FT-IR spectrum showed that the -NH and N-O vibration bands are still present in AO-COF-ben and AO-COF-tri (**Figure S14**), indicating that the amidoxime moieties remained stable during the successive cycles. Additionally, the FT-IR spectrum for AO-COF-ben and AO-COF-tri adsorbents after adsorption, four new vibrations have appeared (**Figure 3d**). More specifically, the vibrations at 1547 cm^{-1} and 1345 cm^{-1} correspond to the symmetric and asymmetric vibrations of $-NO_2$, the bands at 1097 cm^{-1} and 863 cm^{-1} can be assigned to the stretching vibration of C-As and As-O, respectively[28]. All these signals originate from ROX. However, these ROX-originated vibrations disappeared in the regenerated AO-COF-ben and AO-COF-tri materials, which imply that the amidoxime-functionalized COFs can be regenerated by simply washing with a 1 M Na_2CO_3 desorption solution. Additionally, after five cycles, the PXRD patterns of the COFs show no significant changes in comparison to the fresh adsorbents, suggesting that the crystal structure of AO-COF-ben and AO-COF-tri remained intact (**Figure S15**).

Natural water consists of complex ingredients, including various kinds of inorganic ions, dissolved organic matter, and microorganisms, which may affect the adsorption process. To examine if AO-COF-ben and AO-COF-tri could efficiently adsorb ROX in the presence of interfering compounds, river-water, lake-water, and seawater were used to evaluate the adsorption efficiency of the two amidoxime-functionalized COFs. The effect of natural water on the adsorption efficiency of the two amidoxime-functionalized COFs for ROX was investigated by an adsorption experiment with various concentrations of ROX. As shown in **Figure S16**, the adsorption efficiency could reach at least 99 % on both of the two amidoxime-functionalized COFs. These results show that the adsorption of ROX, even present in

low concentrations, is hardly affected by the presence of inorganic ions, dissolved organic matter, and microorganisms.

In order to obtain insights into the adsorption mechanism, electrostatic interactions, hydrogen bonding, and π-π interactions were taken into consideration. To investigate the role of the electrostatic interactions during ROX adsorption, the equilibrium adsorption capacity of the two amidoxime-functionalized COFs at different acidities (pH 2-10) was investigated. As illustrated in **Figure S17**, when the pH was below 5, the adsorption capacity increased with increasing pH and reached the highest adsorption capacity at pH=4, after which it decreased slowly. Meanwhile, the zeta potential shows that the isoelectric points of both the AO-COF-ben and AO-COF-tri is approximately pH=6.7 (**Figure S17**). Additionally, ROX can form charged species with pKa values of 3.49, 5.74, and 9.13 (**Scheme 1**). Based on this, if electrostatic interactions are the dominant factor during adsorption, the highest adsorption efficiency for ROX on the amidoxime-functionalized COFs should occur at 3.49 < pH < 6.7, because of the opposite charges of the COFs and the ROX molecule to attract each other. Moreover, the adsorption efficiency should be negligible at pH < 3.49 or pH > 6.7, because of the same charge of the COFs and ROX, which leads to mutual exclusion. However, the experimental results are not in accordance with these findings, suggesting that the main factor for adsorption does not involve electrostatic interactions. Similar conclusions were obtained for the adsorption of phenylarsonic acid (PAA) and *p*-ASA on MIL-101(OH)$_3$[29].

In order to investigate the intermolecular hydrogen bonding between the amidoxime-functionalized COFs and ROX, ROX adsorbed by AO-COF-tri under different pHs were analyzed by FT-IR spectroscopy. As illustrated in **Figure S18**, our focus was on the vibration band around 3378 cm^{-1}, which corresponds to the -OH

stretching vibration. While decreasing the pH, a shift in the band from 3378 to 3368, 3364, 3359, and 3354 cm^{-1} was observed after the adsorption of ROX onto AO-COF-tri. That of AO-COF-ben has the same trend. This decrease in wavenumber can be attributed to the attachment of ROX onto the -OH stretching. Or in other words, it means that there is an intermolecular hydrogen bond between amidoxime-functionalized COFs and ROX additionally. The π-π electron donor-acceptor interactions were also considered as one of the predominant driving forces for the adsorption of organic chemicals on amidoxime-functionalized COFs[27-28]. To elucidate the role of the π-π electron donor-acceptor interactions in amidoxime-functionalized COFs for ROX adsorption, the molecular level DFT calculation was employed. As shown in **Figure S19**, the adsorption energy of π-π interaction for AO-COF-ben and AO-COF-tri towards ROX is −42.36 kJ/mol and −56.87 kJ/mol, respectively. (face-face distance, 3.4 Å and 2.8 Å) indicating that π-π stacking plays also an important role in the adsorption process. Moreover, the adsorption energy of AO-COF-tri is higher than that of AO-COF-ben. This is because AO-COF-tri has a planar structure, so better stacking can occur. This explains why AO-COF-tri exhibits a higher adsorption capacity for ROX than AO-COF-ben[26]. In conclusion, ROX would form monolayer adsorption on the surface of amidoxime-functionalized COFs, under the combined interactions of intermolecular hydrogen bonding and π-π electron donor-acceptor interactions.

Conclusion

In summary, two highly crystalline and porous amidoxime-functionalized COFs have been successfully prepared via PSM. The usage of COFs as fluorescence sensors and adsorbents towards the detection and adsorption of organic arsenic from water has been investigated for the first time. Due to the long-range order, π-conjugated system,

and adjustable active adsorption sites, both COFs acted as good fluorescent sensors and adsorbents towards the detection and removal of ROX. The fluorescence quenching efficiencies of ROX on both COFs are up to 99%. The limits of detection (LOD) towards ROX are estimated to be 6.5 nM and 12.3 nM. Meanwhile, the abundant active adsorption sites on the open channels of those two COFs facilitate the adsorption of ROX. The adsorption capacity is 732 and 787 mg/g. Such excellent detection and adsorption properties of the amidoxime-functionalized COFs demonstrate their great potential for ROX detection and adsorption from water.

Acknowledgments

H.C. and W.L.L. gratefully acknowledge the Chinese Scholarship Council (CSC) for financial support (201808110210, 201804910742). M. M. gratefully acknowledges the Verbundvorhaben iNEW: Inkubator Nachhaltige Elektrochemische Wertschöpfungsketten with the funding number 03SF0589A for financial support. K.L and P.V.D.V acknowledge the support from the Research Board of Ghent University (GOA010-17, BOF GOA2017000303).

References:

[1] aP. Ravenscroft, H. Brammer, K. Richards, *Arsenic pollution: a global synthesis, Vol. 94*, John Wiley & Sons, **2011**; bR. Quansah, F. A. Armah, D. K. Essumang, I. Luginaah, E. Clarke, K. Marfoh, S. J. Cobbina, E. Nketiah-Amponsah, P. B. Namujju, S. Obiri, *Environmental health perspectives* **2015**, *123*, 412-421; cJ. Luo, Z. Qiu, J. a. Chen, L. Zhang, W. Liu, Y. Tan, W. Shu, *Toxicology* **2013**, *311*, 99-106; dM. Tolins, M. Ruchirawat, P. Landrigan, *Annals of global health* **2014**, *80*, 303-314.

[2] aD. Mohan, C. U. Pittman Jr, *Journal of hazardous materials* **2007**, *142*, 1-53; bC. Wang, J. Luan, C. Wu, *Water research* **2019**, *158*, 370-382; cR. Amen, H. Bashir, I. Bibi, S. M. Shaheen, N. K. Niazi, M. Shahid, M. M. Hussain, V. Antoniadis, M. B. Shakoor, S. G. Al-Solaimani, *Chemical Engineering Journal* **2020**, *396*, 125195; dN. R. Nicomel, K. Leus, K. Folens, P. Van Der Voort, G. Du Laing, *International journal of environmental research and public health* **2016**, *13*, 62.

[3] aW.-R. Chen, C.-H. Huang, *Journal of hazardous materials* **2012**, *227*, 378-385; bS. Depalma,

S. Cowen, T. Hoang, H. A. Al-Abadleh, *Environmental science & technology* **2008**, *42*, 1922-1927; cB. P. Jackson, P. Bertsch, M. Cabrera, J. Camberato, J. Seaman, C. Wood, *Journal of environmental quality* **2003**, *32*, 535-540.

[4] aA. Adak, K. P. Mangalgiri, J. Lee, L. Blaney, *Water research* **2015**, *70*, 74-85; bL. Wang, H. Cheng, *Environmental science & technology* **2015**, *49*, 3473-3481.

[5] F.-M. Wang, Z.-L. Chen, L. Zhang, Y.-L. Gao, Y.-X. Sun, *Plant and soil* **2006**, *285*, 359-367.

[6] J. Hu, Z. Tong, Z. Hu, G. Chen, T. Chen, *J Colloid Interface Sci* **2012**, *377*, 355-361.

[7] Y. Jiang, Y. Liu, Y. Zhang, Y. Chen, X. Zan, *Nanomaterials* **2020**, *10*, 1765.

[8] L. Poon, S. Younus, L. D. Wilson, *Journal of colloid and interface science* **2014**, *420*, 136-144.

[9] A. R. Roerdink, J. H. Aldstadt III, *Journal of chromatography A* **2004**, *1057*, 177-183.

[10] B. P. Jackson, P. M. Bertsch, *Environmental Science & Technology* **2001**, *35*, 4868-4873.

[11] J. Cui, Y.-b. Xiao, L. Dai, X.-h. Zhao, Y. Wang, *Food Analytical Methods* **2013**, *6*, 370-379.

[12] A. P. Demchenko, *Introduction to fluorescence sensing*, Springer Science & Business Media, **2008**.

[13] aJ. L. Segura, M. J. Mancheno, F. Zamora, *Chem Soc Rev* **2016**, *45*, 5635-5671; bP. Van Der Voort, H. Chen, W. Liu, A. Laemont, C. Krishnaraj, X. Feng, F. Rohman, Q. Zhang, M. Meledina, r. van deun, *Angewandte Chemie* **2021**; cM. S. Lohse, T. Bein, *Advanced Functional Materials* **2018**, *28*, 1870229.

[14] aH. Ding, A. Mal, C. Wang, *Materials Chemistry Frontiers* **2020**, *4*, 113-127; bJ. L. Segura, S. Royuela, M. M. Ramos, *Chemical Society Reviews* **2019**, *48*, 3903-3945.

[15] aX. Wu, X. Han, Q. Xu, Y. Liu, C. Yuan, S. Yang, Y. Liu, J. Jiang, Y. Cui, *J Am Chem Soc* **2019**, *141*, 7081-7089; bZ. Li, N. Huang, K. H. Lee, Y. Feng, S. Tao, Q. Jiang, Y. Nagao, S. Irle, D. Jiang, *J Am Chem Soc* **2018**, *140*, 12374-12377; cL. Chen, L. He, F. Ma, W. Liu, Y. Wang, M. A. Silver, L. Chen, L. Zhu, D. Gui, J. Diwu, Z. Chai, S. Wang, *ACS Appl Mater Interfaces* **2018**, *10*, 15364-15368; dH. L. Qian, C. Dai, C. X. Yang, X. P. Yan, *ACS Appl Mater Interfaces* **2017**, *9*, 24999-25005.

[16] M. Faheem, S. Aziz, X. Jing, T. Ma, J. Du, F. Sun, Y. Tian, G. Zhu, *Journal of Materials Chemistry A* **2019**, *7*, 27148-27155.

[17] aM. Yang, C. Mo, L. Fang, J. Li, Z. Yuan, Z. Chen, Q. Jiang, X. Chen, D. Yu, *Advanced Functional Materials* **2020**, *30*; bY. Zhao, H. Liu, C. Wu, Z. Zhang, Q. Pan, F. Hu, R. Wang, P. Li, X. Huang, Z. Li, *Angew Chem Int Ed Engl* **2019**, *58*, 5376-5381.

[18] C.-R. Zhang, W.-R. Cui, W. Jiang, F.-F. Li, Y.-D. Wu, R.-P. Liang, J.-D. Qiu, *Environmental Science: Nano* **2020**, *7*, 842-850.

[19] Y. Zhao, Z. Sui, Z. Chang, S. Wang, Y. Liang, X. Liu, L. Feng, Q. Chen, N. Wang, *Journal of Materials Chemistry A* **2020**, *8*, 25156-25164.

[20] S. Bi, C. Yang, W. Zhang, J. Xu, L. Liu, D. Wu, X. Wang, Y. Han, Q. Liang, F. Zhang, *Nature communications* **2019**, *10*, 1-10.

[21] Z. Xiang, D. Cao, *Macromol Rapid Commun* **2012**, *33*, 1184-1190.

[22] W. K. Haug, E. M. Moscarello, E. R. Wolfson, P. L. McGrier, *Chemical Society Reviews* **2020**, *49*, 839-864.

[23] J. W. Jun, M. Tong, B. K. Jung, Z. Hasan, C. Zhong, S. H. Jhung, *Chemistry* **2015**, *21*, 347-354.

[24] B. Li, X. Zhu, K. Hu, Y. Li, J. Feng, J. Shi, J. Gu, *J Hazard Mater* **2016**, *302*, 57-64.

[25] Y. Xu, J. Lv, Y. Song, X. Zhou, C. Tian, X. Hong, Y. Cai, C. Zhao, Z. Lin, *Environmental Science: Nano* **2019**, *6*, 3590-3600.

[26] J. Dong, Y. Wang, G. Liu, Y. Cheng, D. Zhao, *CrystEngComm* **2017**, *19*, 4899-4904.
[27] C. Tian, J. Zhao, X. Ou, J. Wan, Y. Cai, Z. Lin, Z. Dang, B. Xing, *Environ Sci Technol* **2018**, *52*, 3466-3475.
[28] Y. Lv, R. Zhang, S. Zeng, K. Liu, S. Huang, Y. Liu, P. Xu, C. Lin, Y. Cheng, M. Liu, *Chemical Engineering Journal* **2018**, *339*, 359-368.
[29] M. Sarker, J. Y. Song, S. H. Jhung, *J Hazard Mater* **2017**, *335*, 162-169.